AD-A043 199 STANFORD RESEARCH INST MENLO PARK CALIF F/G 19/1
SIMULATION OF EARTH PENETRATION LOADS.(U)
SEP 76 J D COLTON, R E EMERSON, H E LINDBERG DNA001-75-C-0257
UNCLASSIFIED DNA-4141F NL

| OF |
ADA
043199

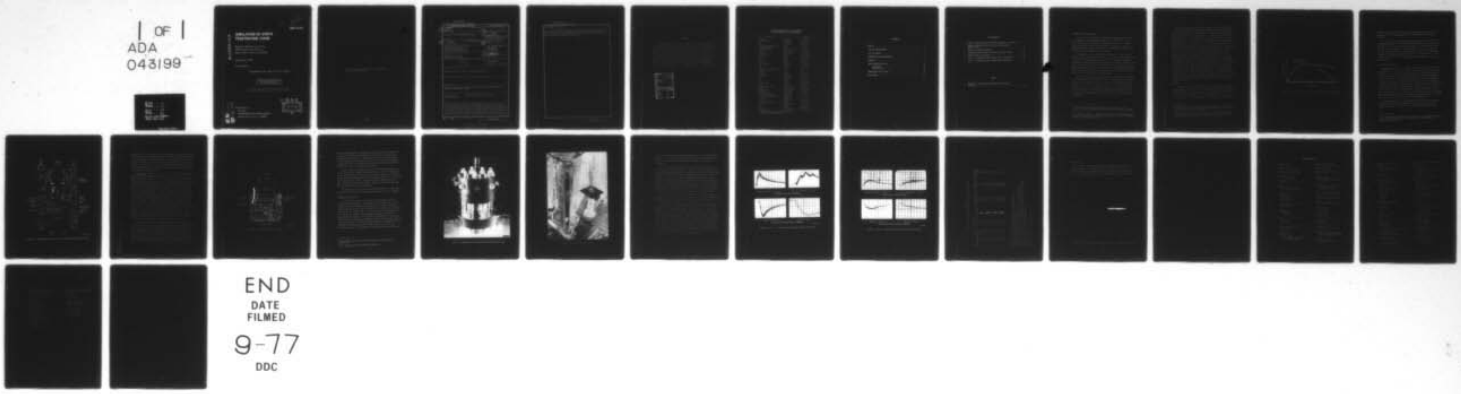

END
DATE
FILMED
9-77
DDC

(10)

DNA 4141F

AD A043199

SIMULATION OF EARTH PENETRATION LOADS

Stanford Research Institute
333 Ravenswood Avenue
Menlo Park, California 94025

September 1976

Final Report

CONTRACT No. DNA 001-75-C-0257

THIS WORK SPONSORED BY THE DEFENSE NUCLEAR AGENCY
UNDER RDT&E RMSS CODE B342075464 N99QAXAA13014 H2590D.

Prepared for
Director
DEFENSE NUCLEAR AGENCY
Washington, D. C. 20305

Destroy this report when it is no longer needed.
Do not return to sender.

UNCLASSIFIED

SECURITY CLASSIFICATION OF THIS PAGE (When Data Entered)

REPORT DOCUMENTATION PAGE

READ INSTRUCTIONS BEFORE COMPLETING FORM

1. REPORT NUMBER: DNA 4141F	2. GOVT ACCESSION NO.
3. RECIPIENT'S CATALOG NUMBER	
4. TITLE (and Subtitle): SIMULATION OF EARTH PENETRATION LOADS.	5. TYPE OF REPORT & PERIOD COVERED: Final Report
6. PERFORMING ORG. REPORT NUMBER: SRI Project PYU 4149	
7. AUTHOR(s): J. D. Colton, H. E. Lindberg (Supervisor), R. E. Emerson	8. CONTRACT OR GRANT NUMBER(s): DNA 001-75-C-0257
9. PERFORMING ORGANIZATION NAME AND ADDRESS: Stanford Research Institute, 333 Ravenswood Avenue, Menlo Park, California 94025	10. PROGRAM ELEMENT, PROJECT, TASK AREA & WORK UNIT NUMBERS: NWED Subtask N99QAXAA130-14
11. CONTROLLING OFFICE NAME AND ADDRESS: Director, Defense Nuclear Agency, Washington, D.C. 20305	12. REPORT DATE: September 1976
	13. NUMBER OF PAGES: 26
14. MONITORING AGENCY NAME & ADDRESS (if different from Controlling Office)	15. SECURITY CLASS (of this report): UNCLASSIFIED
	15a. DECLASSIFICATION/DOWNGRADING SCHEDULE

16. DISTRIBUTION STATEMENT (of this Report)

Approved for public release; distribution unlimited.

17. DISTRIBUTION STATEMENT (of the abstract entered in Block 20, if different from Report)

18. SUPPLEMENTARY NOTES

This work sponsored by the Defense Nuclear Agency under RDT&E RMSS Code B342075464 N99QAXAA13014 H2590D.

19. KEY WORDS (Continue on reverse side if necessary and identify by block number)

Load Simulation
Earth Penetration
Shallow Burst Munitions Structures

20. ABSTRACT (Continue on reverse side if necessary and identify by block number)

An experimental apparatus was developed to simulate the impact loads on earth penetrating structures. The device has been built to test ¼-scale model structures, but the design is suitable for fabrication in a larger size for testing full-scale structures. The device uses the controlled flow of high-pressure explosion product gases acting against a piston to apply either an axial load or combined axial and lateral loads to a model structure. Loading parameters such as rise time and peak load can be easily varied from

DD FORM 1 JAN 73 1473 EDITION OF 1 NOV 65 IS OBSOLETE

UNCLASSIFIED

SECURITY CLASSIFICATION OF THIS PAGE (When Data Entered)

20. ABSTRACT (Continued)

test to test by simple adjustments of the device. The technique allows hard-wired measurement of the applied load and the response of the structure. A series of initial calibration tests conducted without a model structure indicates that the device operates properly.

PREFACE

The original objective of this contract was to devise a means of creating a well-defined dust cloud for testing heat shield materials in dust erosion. This work has been completed and the final report, entitled "The Feasibility of Generation of Linear Particulate Clouds," has been submitted. The contract has been modified to include a task to develop a technique for simulating the impact loads on earth penetrating structures. This final report describes the experimental apparatus constructed for that purpose and some initial test results. The contract monitor was Mr. M. J. Rubenstein of DNA. Technical assistance was also provided by Lt. R. Nibe of DNA.

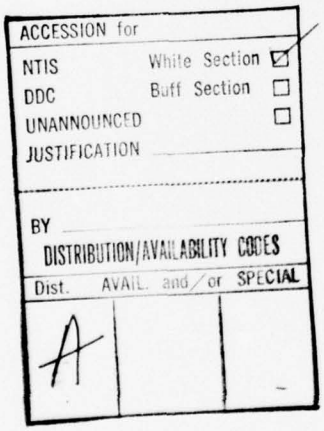

Conversion factors for U.S. customary to metric (SI) units of measurement.

To Convert From	To	Multiply By
angstrom	meters (m)	1.000 000 X E -10
atmosphere (normal)	kilo pascal (kPa)	1.013 25 X E +2
bar	kilo pascal (kPa)	1.000 000 X E +2
barn	meter^2 (m^2)	1.000 000 X E -28
British thermal unit (thermochemical)	joule (J)	1.054 350 X E +3
calorie (thermochemical)	joule (J)	4.184 000
cal (thermochemical)/cm^2	mega joule/m^2 (MJ/m^2)	4.184 000 X E -2
curie	*giga becquerel (GBq)	3.700 000 X E +1
degree (angle)	radian (rad)	1.745 329 X E -2
degree Fahrenheit	degree kelvin (K)	$t_K = (t°f + 459.67)/1.8$
electron volt	joule (J)	1.602 19 X E -19
erg	joule (J)	1.000 000 X E -7
erg/second	watt (W)	1.000 000 X E -7
foot	meter (m)	3.048 000 X E -1
foot-pound-force	joule (J)	1.355 818
gallon (U.S. liquid)	meter^3 (m^3)	3.785 412 X E -3
inch	meter (m)	2.540 000 X E -2
jerk	joule (J)	1.000 000 X E +9
joule/kilogram (J/kg) (radiation dose absorbed)	Gray (Gy)	1.000 000
kilotons	terajoules	4.183
kip (1000 lbf)	newton (N)	4.448 222 X E +3
kip/inch^2 (ksi)	kilo pascal (kPa)	6.894 757 X E +3
ktap	newton-second/m^2 ($N-s/m^2$)	1.000 000 X E +2
micron	meter (m)	1.000 000 X E -6
mil	meter (m)	2.540 000 X E -5
mile (international)	meter (m)	1.609 344 X E +3
ounce	kilogram (kg)	2.834 952 X E -2
pound-force (lbs avoirdupois)	newton (N)	4.448 222
pound-force inch	newton-meter (N·m)	1.129 848 X E -1
pound-force/inch	newton/meter (N/m)	1.751 268 X E +2
pound-force/foot^2	kilo pascal (kPa)	4.788 026 X E -2
pound-force/inch^2 (psi)	kilo pascal (kPa)	6.894 757
pound-mass (lbm avoirdupois)	kilogram (kg)	4.535 924 X E -1
pound-mass-foot^2 (moment of inertia)	kilogram-meter^2 ($kg \cdot m^2$)	4.214 011 X E -2
pound-mass/foot^3	kilogram/meter^3 (kg/m^3)	1.601 846 X E +1
rad (radiation dose absorbed)	**Gray (Gy)	1.000 000 X E -2
roentgen	coulomb/kilogram (C/kg)	2.579 760 X E -4
shake	second (s)	1.000 000 X E -8
slug	kilogram (kg)	1.459 390 X E +1
torr (mm Hg, 0° C)	kilo pascal (kPa)	1.333 22 X E -1

*The becquerel (Bq) is the SI unit of radioactivity; 1 Bq = 1 event/s.
**The Gray (Gy) is the SI unit of absorbed radiation.

CONTENTS

ILLUSTRATIONS

TABLE

INTRODUCTION AND BACKGROUND

As part of the development of earth-penetrating weapons, the impact response of the penetrator casing must be understood so that it can be designed to stay intact and allow penetration of the target to the required depth. This report describes the work under contract DNA001-75-C-0257, in which a technique for simulating the impact loads on earth penetrator structures was developed.*

The immediate use for a simulation technique is to apply well-defined loads to scale model structures. The response data obtained can be used to verify mathematical analysis of the penetrator response. A simulation technique would also be useful for loading full-scale structures in the elastic range so that many tests could be performed on a single structure. Therefore, the design of the loading device developed here for scale model structures was made suitable for fabrication in a larger size for loading full-scale structures.

For angle of attack impacts, large strains and failures in penetrator structures have been observed to occur at distances greater than one diameter from the penetrator nose.† The stress distribution over the cross-section at these locations depends only on the resultant forces applied to the end of the structure. Thus, the simulation technique need only produce the resultant axial and lateral loading forces with the appropriate time-history but need not produce a particular load distribution.

---

*Further testing using this technique, and an analysis of the impact response, are being performed under Contract DNA001-74-C-0140.

†M. L. Anthony, "Impact of Earth Penetrator Models into Simulated Rock Targets," Martin Marietta Aerospace Company, Final Report for Contract DNA001-75-C-0161, November 1975.

Both calculated impact loads* and measured acceleration response† show that the resultant force-history for normal impact consists of two distinct parts, as Figure 1 illustrates: an approximately linear rise to a peak over the time τ_1 required for the structure to penetrate to its full diameter, and a very gradual decay associated with the rigid body deceleration of the structure. For a nominal full-scale structure [6 in. (15.24 cm) in diameter, 60 in. (152.4 cm) long, and weighing 400 lbs. (181 kg)] impacting sandstone at 1500 ft/sec (457 m/sec), the loading rise time is about 1 msec and the peak force is about 500,000 lbs. (2224 kN). For impacts with nonzero angle of obliquity or angle of attack, a lateral force is also applied to the structure. In the simulation technique described here, it was assumed that the lateral load is proportional to the axial load (i.e., that F_L/F_A is constant with respect to time). Since an earth penetrating structure would fail during the load rise time or at about the time the load reaches its peak, the simulation technique must produce the axial and lateral loading forces until they reach their peak values. A simulated impact load history, in the axial or lateral direction, is illustrated in Figure 1, which shows a linear increase in amplitude during τ_1, a constant or slowly decaying history after the peak value for a time τ_2, and a decay over a time τ_3.

APPROACH

A load simulation device to meet these requirements was developed for a nominal scale factor of 1/4. For this scale factor, a device was designed to produce a simulated load such as that shown in Figure 1 within the nominal ranges: $0 \leq F_o \leq 35{,}000$ lb. (155,700 N), $100 < \tau_1 < 500$ μsec, $100 < \tau_2 < 200$ μsec, $300 < \tau_3 < 1000$ μsec. These loads are

---

*"Internal Response in Earth Penetrators," Presented by K. Kreyenhagen, California Research and Technology, at the DNA Earth Penetration Technology Review Meeting, October 1975.

†Paul F. Hadala, "Evaluation of Empirical and Analytical Procedures Used for Predicting the Rigid Body Motion of an Earth Penetrator," Waterways Experimental Station Paper S-75-15, June 1975.

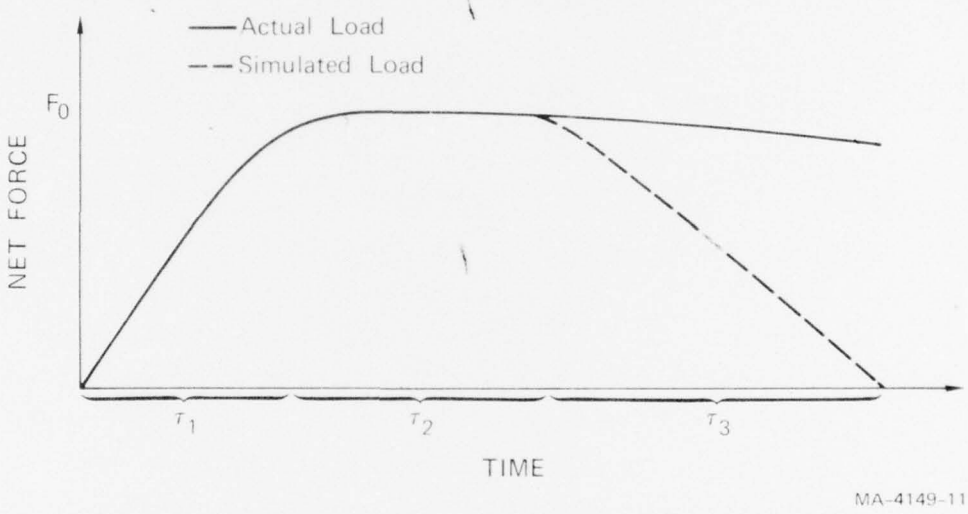

FIGURE 1 IMPACT LOAD-TIME HISTORY ON EARTH-PENETRATOR STRUCTURES

produced with an explosive loading technique similar to that used successfully in other applications where a prescribed load history was required.

In the current load-simulation application, the controlled flow of high-pressure gases from a confined explosion produces the desired pressure pulse in a cylinder containing a piston. The piston transmits the load to the model structure. Since the model structure is initially at rest, the total kinetic energy associated with this load-simulation technique is substantially less than that of reverse ballistics. Also, starting the model at rest allows hard-wired measurement of the loads and strains.

LOAD SIMULATION DEVICE

Operation--Figure 2 is a sectioned assembly drawing of the fixture in configuration for simulating normal impact loads on 1/4-scale model penetrators. The fixture operates as follows: high-pressure gaseous explosive products are produced in the explosive chamber by detonation of a solid explosive. The gas flows through an orifice plate and into a cylinder containing a piston that is in contact with the penetrator. The load is transmitted to the penetrator through the piston (the details of this interface are discussed later). The rise time τ_1 of the load can be varied by using different initial piston displacements or different orifice areas. The duration τ_2 of the constant load can be varied by using vent holes at different locations along the cylinder. The decay time τ_3 can be varied by using different size vent holes.

The pulse produced by a given geometry may be predicted using the GASLEAK computer code* that models the flow of gases in a series of chambers connected by orifices. The theoretical model of the flow

---

*D. J. Cagliostro, "Experiments on the Response of Hexagonal Subassembly Ducts to Radial Loads," SRI Interim Report for Argonne National Laboratory, August 1975.

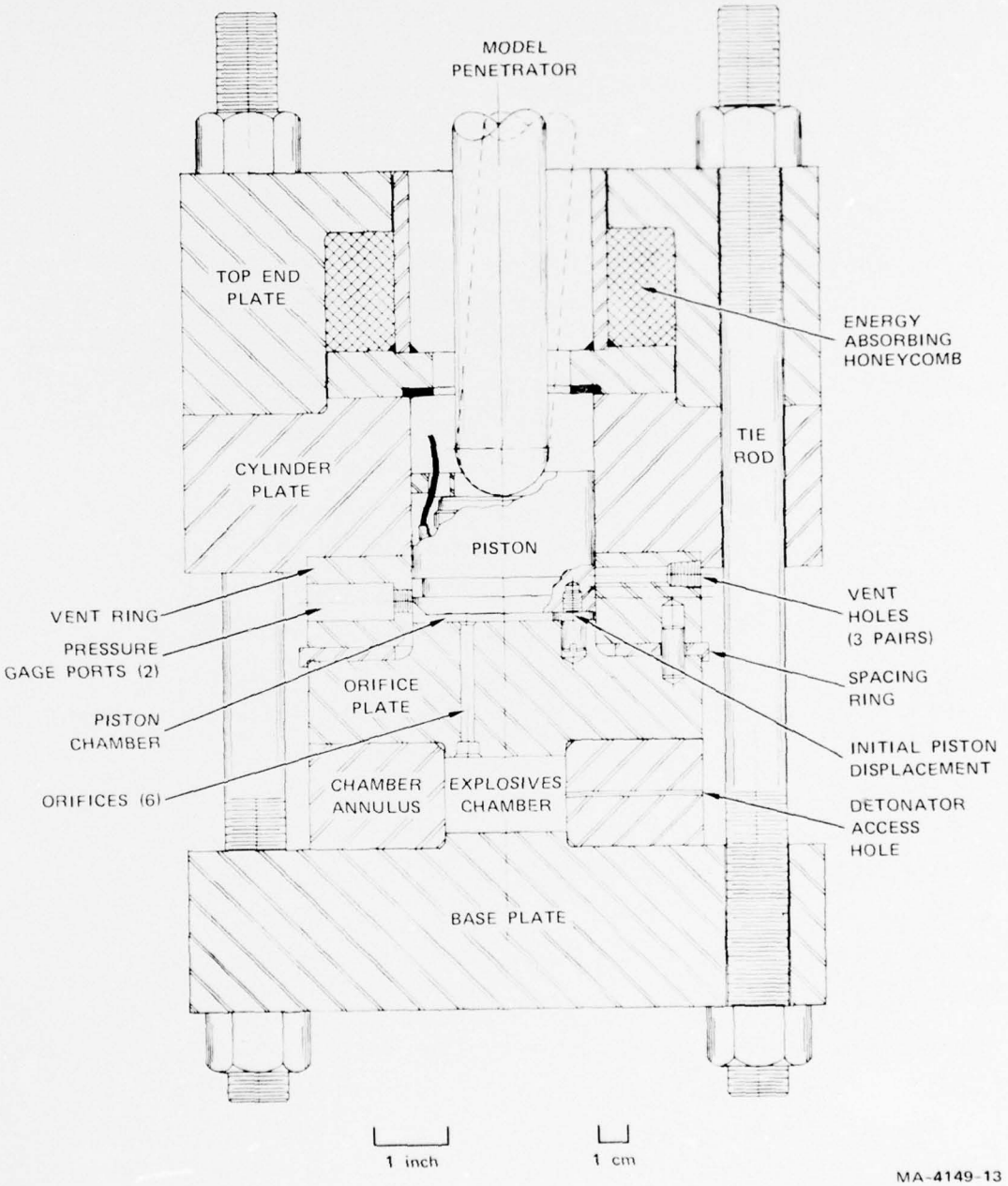

FIGURE 2 ASSEMBLY DRAWING OF TEST FIXTURE FOR SIMULATING IMPACT LOADS

assumes that (1) the duration of the loading pulse is long compared with the transit time of pressure waves in each chamber (quasi-steady flow); (2) negligible heat is transferred from the hot gas to the surrounding cylinder (adiabatic flow); (3) the hot detonation products behave as a perfect gas. Experience in other similar applications has shown excellent agreement between the theoretically predicted pressure pulse and the experimentally measured pulse.

Construction--The device is constructed of a stack of alloy steel rings and circular plates clamped together by eight tie rods. The explosive chamber is formed by a thick-walled annulus that fits between the base plate and the orifice plate. The cross-sectional area of each of the six orifices may be varied by inserting plugs drilled with the proper size hole into the recesses on the lower side of the orifice plate. The cylinder in which the piston travels is formed by the vent ring and the cylinder plate. The initial volume of the piston chamber is controlled by a spacing washer between the piston and orifice plate, which sets the initial piston displacement. The vent ring has three pairs of vent holes, each pair at a different axial location. These holes vent the piston chamber to the atmosphere as the piston passes. The size of the vent area may be varied with threaded plugs that reduce the area of the vent holes or close the holes completely. The axial location of the holes is set by the thickness of the spacing ring. Two pressure gages are mounted diametrically opposed in the vent ring to measure the chamber pressure. After the pulse is produced, the piston decelerates by impacting the energy-absorbing aluminum honeycomb.

To simulate the load on a penetrator that impacts at an angle of attack, the piston is designed to produce both axial and lateral loading and to measure directly the resultant load applied to the penetrator. The combined loading is produced by tilting the penetrator through an angle θ with respect to the piston axis, as shown in the sectioned drawing of the piston in Figure 3. The vertical force F is measured with a piezoelectric load cell (Kistler 906A). Two discs are placed between the load cell and the penetrator and the interface between

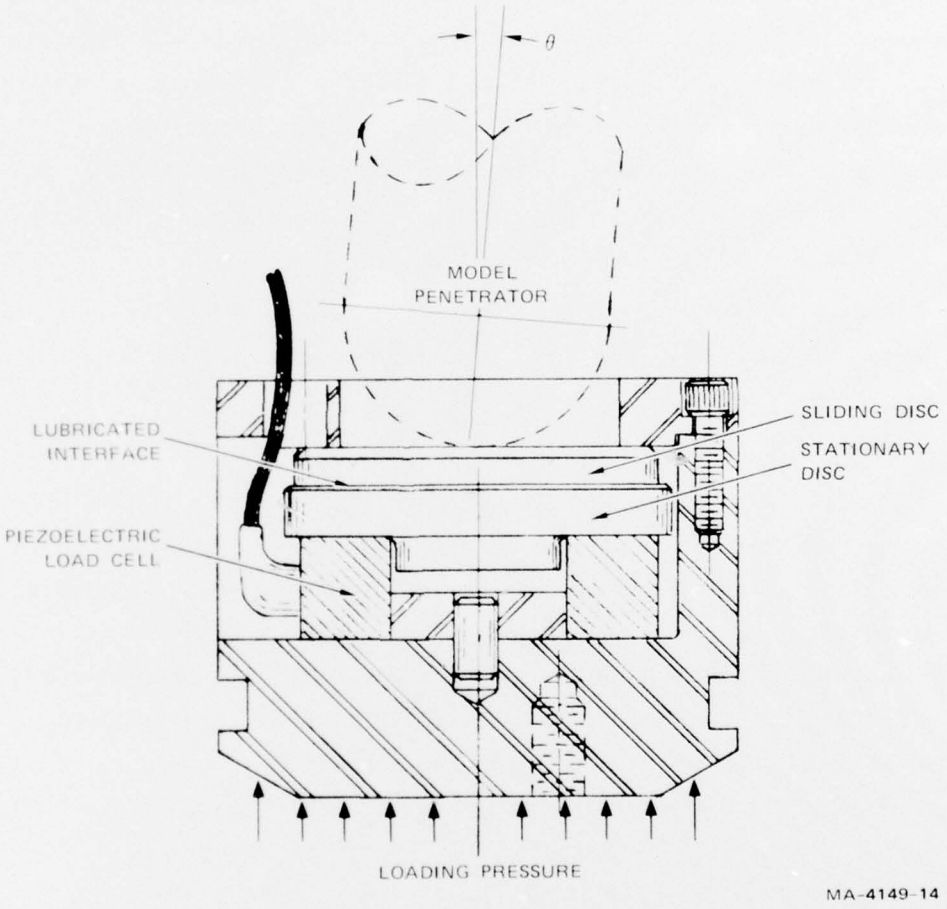

FIGURE 3 PISTON FOR ANGULAR LOADING

them is lubricated with a high-pressure, low-friction solid lubricant* to minimize frictional forces parallel to the face of the load cell. By allowing the loaded end of the penetrator to slide across the load cell with negligible friction forces, the vertical force F is parallel to the piston axis. The axial load applied to the model SBM structure is then $F \cdot \cos\theta$, and the lateral load is $F \cdot \sin\theta$.

Figure 4 shows the assembled device with a scale model SBM structure in position for a normal impact simulation. After the load simulation, the penetrator leaves the device and is stopped by an external energy absorber (aluminum honeycomb or Styrofoam) located in a 5-ft-long (1.52-m-long) safety shroud. The shroud ensures containment of the model penetrator after the simulation. Figure 5 shows the device with the safety shroud in place for testing.

The fixture can also be used to test larger models. In this case, two parts (the piston and the top end plate) would need to be changed.

EXPERIMENTS WITH PISTON

A series of 11 tests was conducted with the loading device but without a model penetrator. The purpose of these tests was to check the operation under simplified conditions and to compare the piston chamber pressure and the rigid body motion of the piston with the motion predicted by the GASLEAK code. In all tests, the high explosive used was a mixture of PETN† and hollow glass microspheres (90% and 10%, respectively, by weight). The explosive was detonated by a mild detonating fuse that entered the explosives chamber through a small hole in the chamber annulus. The piston chamber pressure was measured with two piezoelectric pressure gages (PCB 113A) mounted in the vent ring 180 degrees apart. An accelerometer (Endevco 2225) mounted on the top

---

*Several brands used, most frequently SprayKote, manufactured by Dow Corning.

†PETN ($C_5H_8O_{12}N_4$) pentaerythritol tetranitrate.

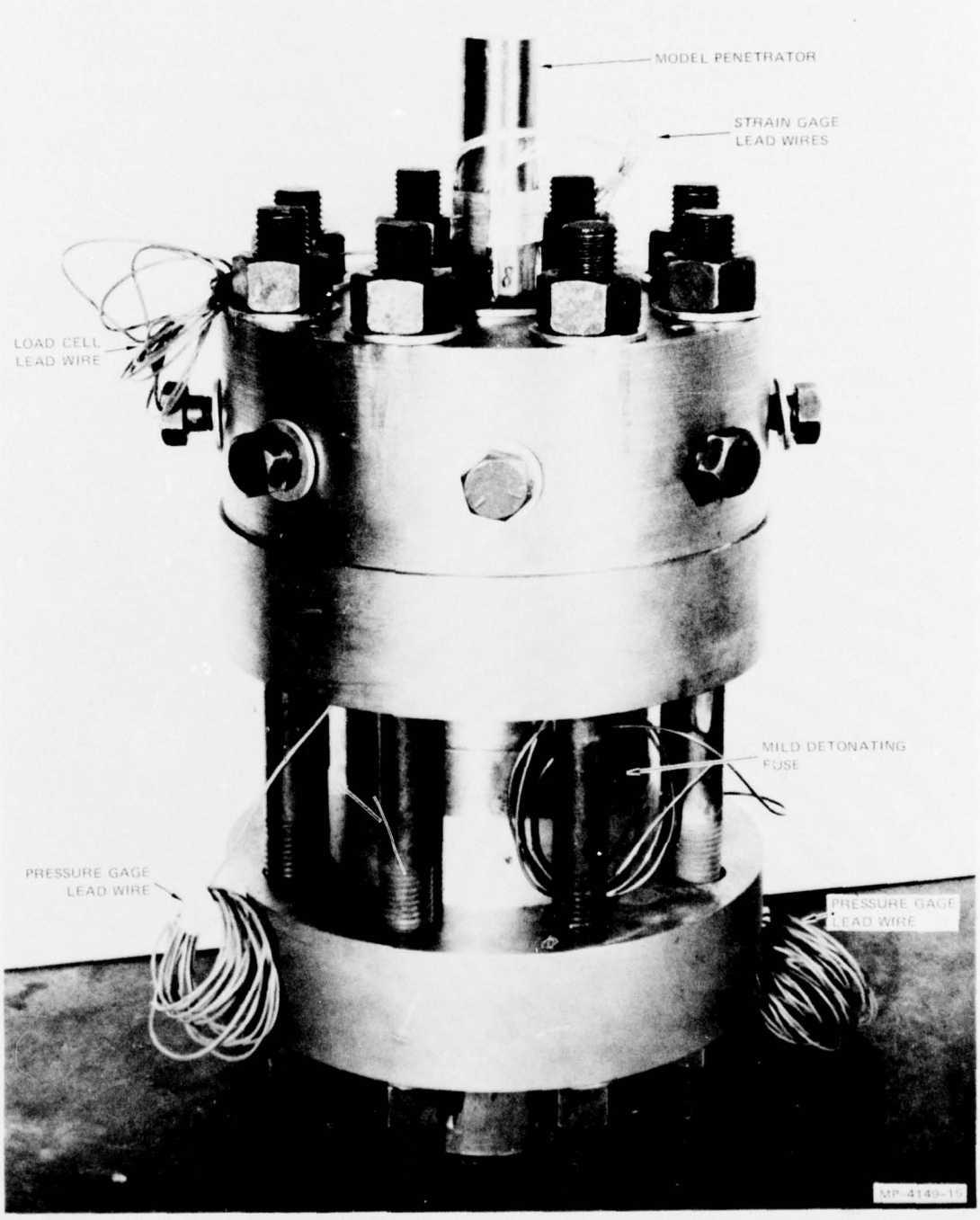

FIGURE 4 ASSEMBLED TEST FIXTURE FOR SIMULATING IMPACT LOADS

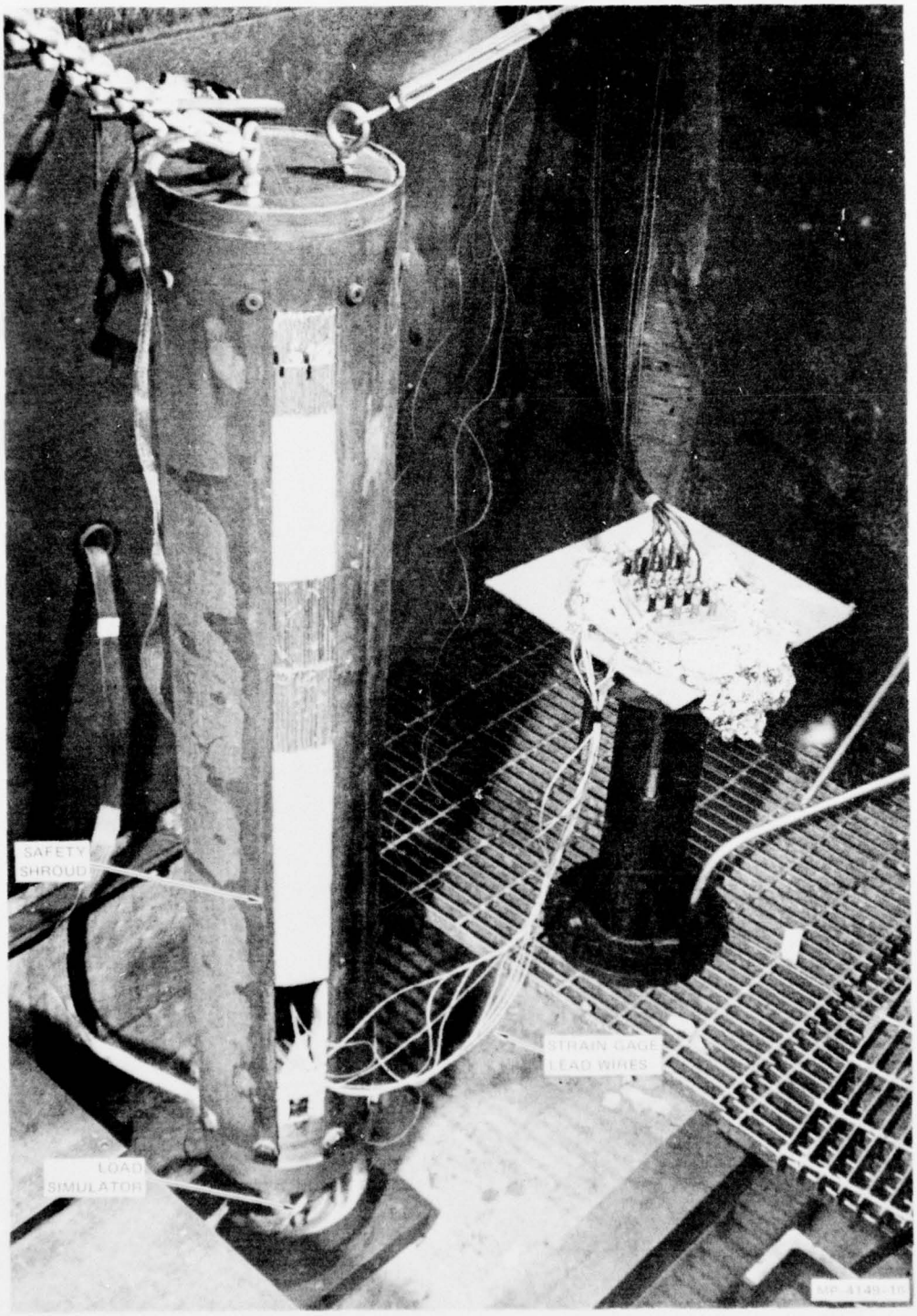

FIGURE 5 FIXTURE READY FOR TESTING

face of the piston recorded the axial acceleration of the piston during the tests. A 1/16-in.-thick (0.16-cm-thick) rubber pad was bonded between the accelerometer and the piston to suppress ringing in the accelerometer.

Figure 6 shows the chamber pressure and piston acceleration in Test 11, without a model penetrator. The device set-up parameters were 1 gram 90/10 PETN/μsphere explosive charge; all orifice plate holes open; 0.060-in. (0.152-cm) initial piston displacement; bottom two pairs of vent holes closed, top pair open; and no spacing ring. The pressure measured at this point oscillates because of pressure waves in the gas, Figure 6(a). However the average pressure over the piston face produces a smooth piston acceleration history, Figure 6(b). The high-frequency oscillations in the acceleration record are caused by the accelerometer and flexible rubber mount vibrating as a simple mass-spring system.

Figure 6 illustrates that, in the absence of a model penetrator, the desired type of pulse is produced: a steep linear rise, an approximately level plateau, and a gradual decay at a rate slower than the rise.

Other tests in the calibration series show that the impact load-time history can be varied by changing the geometry of the device, as described above. For example, Figure 7 shows the results from Test 9 in which the initial piston displacement and explosive charge were increased from those of Test 11. The device set-up parameters for Test 9 were 2 grams 90/10 PETN/μsphere explosive charge; all orifice plate holes open; 0.300-in. (0.762-cm) initial piston displacement; bottom two pairs of vent holes closed, top pair open; and no spacing ring. Comparing Test 9 with Test 11, we see a longer rise time due to the greater initial piston displacement, and higher peak pressure and acceleration due to the larger explosive charge. Table 1 lists the complete series of calibration tests conducted without a model penetrator.

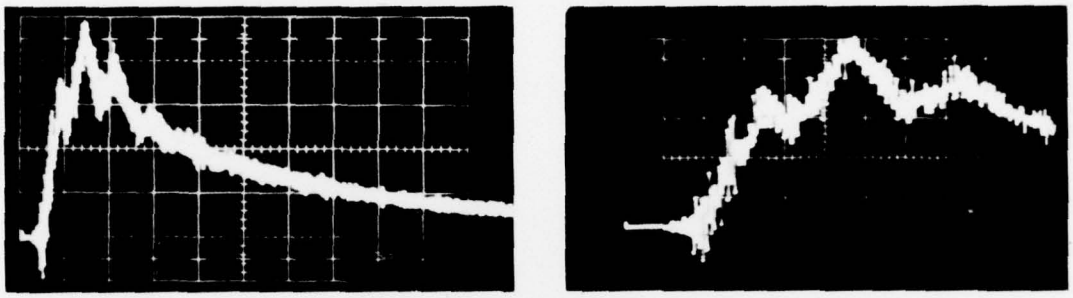

400 psi/cm (2758 kPa/cm) 200 μs/cm

400 psi/cm (2758 kPa/cm) 50 μs/cm

(a) PRESSURE GAGE I (POSITIVE UPWARD)

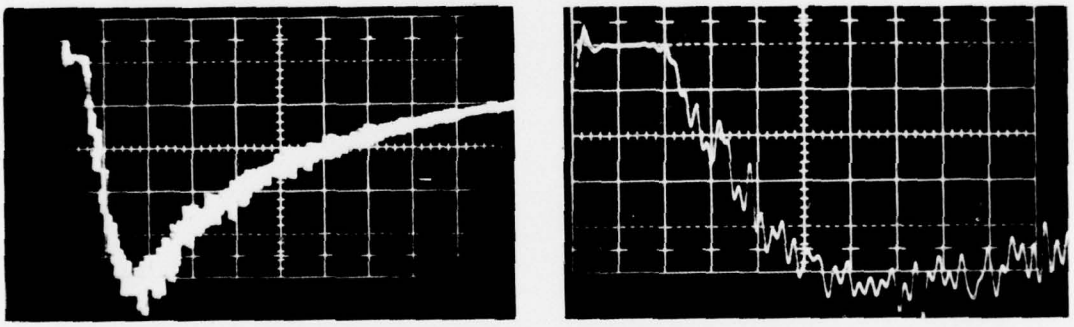

500 g/cm 200 μs/cm

500 g/cm 50 μs/cm

(b) PISTON ACCELERATION (POSITIVE DOWNWARD)

MP-3091-116A

FIGURE 6 TEST 11 – CALIBRATION TEST WITHOUT MODEL PENETRATOR

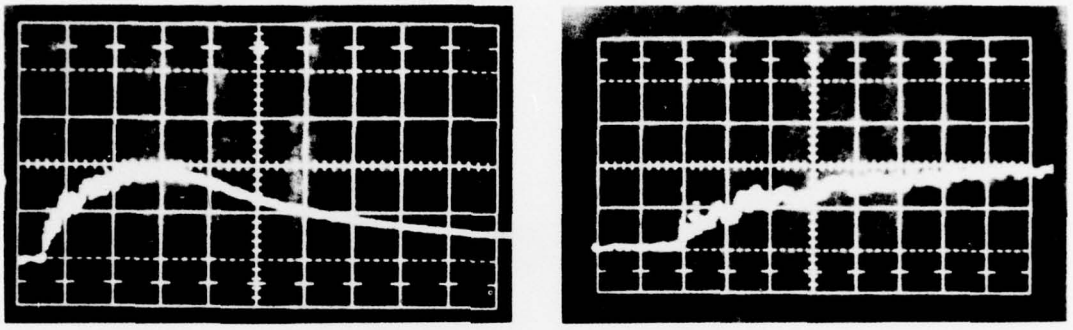

1000 psi/cm (6894 kPa/cm) 200 μs/cm 1000 psi/cm (6894 kPa/cm) 50 μs/cm

(a) PRESSURE GAGE I (POSITIVE UPWARD)

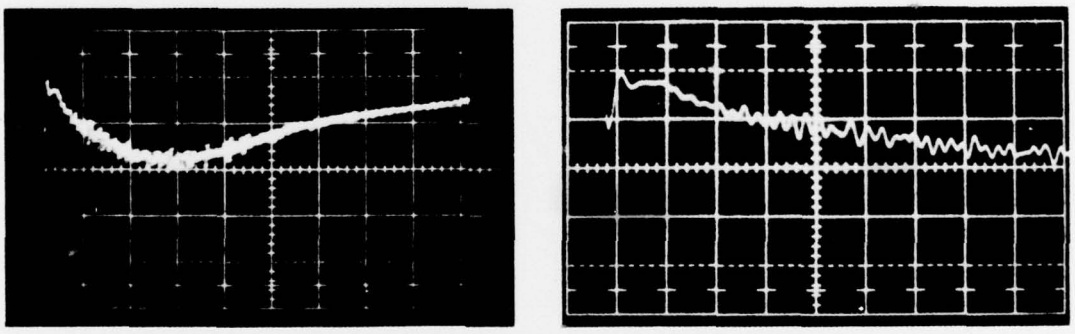

2000 g/cm 200 μs/cm 2000 g/cm 50 μs/cm

(b) PISTON ACCELERATION (POSITIVE DOWNWARD)

MP-4149-17

FIGURE 7 TEST 9—CALIBRATION TEST WITHOUT MODEL PENETRATOR

Table 1

RESULTS OF CALIBRATION EXPERIMENTS WITHOUT MODEL PENETRATOR

Test No.	Date	Charge Mass[a] (gm)	Initial Piston Displacement (cm)	Vent Holes	Peak Pressure[e] (KPa)	Peak Acceleration (g)	Rise Time[g] (μsec)
1	3-12-76	0.66[b]	0.193		5,790	_[f]	_[f]
2	3-15-76	0.66[b]	0.193		6,070	1,700	100
3	3-26-76	0.543	0.457	c	4,140	1,050	180
4	3-26-76	0.543	0.457		3,650	850	170
5	3-29-76	1.086	0.457		7,760	2,000	150
6	3-29-76	1.086	0.457		7,760	2,400	110
7	3-30-76	1.086	0.457		7,070	1,800	135
8	3-30-76	2.00	0.457		14,130	4,000	120
9	3-30-76	2.00	0.762	d	11,720	3,600	240
10	4-02-76	1.00	0.305		7,450	2,000	145
11	4-02-76	1.00	0.152		10,340	2,650	115

[a] For shots 3 through 11, a small (0.02 to 0.05 gram) booster charge (DuPont Detasheet) was used; the mass listed here includes that of 90/10 PETN/usphere charge only.

[b] Includes large (approximately 0.18 gram) booster charge (DuPont Detasheet).

[c] Vent hole configuration: top pair open; middle pair open; bottom pair closed.

[d] Vent hole configuration: top pair open; middle pair closed; bottom pair closed.

[e] Average of the two pressure gage measurements.

[f] Bad gage record.

[g] Time to reach 75% of the peak acceleration.

CONCLUSIONS

The initial results indicate that the apparatus operates as designed. However, to determine whether the loading pulse applied to a structure accurately simulates the expected impact loads, the apparatus needs to be tested with a model earth penetrating structure in place.*

[redacted]

*Additional testing is being performed under Contract DNA001-74-C-0140.

DISTRIBUTION LIST

DEPARTMENT OF DEFENSE

Director
Defense Advanced Research Proj. Agency
ATTN: Strategic Tech. Office

Defense Communication Engineer Center
ATTN: Code 720, John Worthington

Director
Defense Communications Agency
ATTN: NMCSSC, Code 510

Defense Documentation Center
Cameron Station
12 cy ATTN: TC

Director
Defense Intelligence Agency
ATTN: DT-1C, Nuc. Eng. Branch
ATTN: DT-2, Weapons & Sys. Div.
ATTN: DI-7D

Director
Defense Nuclear Agency
3 cy ATTN: TITL, Tech. Library
ATTN: STSP
ATTN: DDST
ATTN: TISI, Archives
ATTN: SPAS
3 cy ATTN: SPSS

Dir. of Defense Research & Engineering
Department of Defense
ATTN: S&SS (OS)

Commander
Field Command
Defense Nuclear Agency
ATTN: FCTMOF
ATTN: FCPR
ATTN: FCTMD

Director
Joint Strat. Target Planning Staff, JCS
ATTN: JPTP
ATTN: JPTM
ATTN: JLTW-2

Chief
Livermore Division, Field Command, DNA
Lawrence Livermore Laboratory
ATTN: FCPRL

DEPARTMENT OF THE ARMY

Program Manager
BMD Program Office
ATTN: DACS-BMZ
ATTN: DACS-BMT, Clifford E. McLain
ATTN: DACS-BMZ-D, Julian Davidson
ATTN: DACS-BMT, John Shea

DEPARTMENT OF THE ARMY (Continued)

Dep. Chief of Staff for Research Dev. & Acq.
Department of the Army
ATTN: NCB Division

Deputy Chief of Staff for Ops. & Plans
Department of the Army
ATTN: Dir. of Nuc. Plans & Policy

Commander
Harry Diamond Laboratories
ATTN: DRXDO-RBH, James H. Gwaltney
ATTN: DRXDO-RC, Robert B. Oswald, Jr.
ATTN: DRXDO-NP

Director
US Army Ballistic Research Labs.
ATTN: DRXRD-BVL, William J. Schuman, Jr.
ATTN: DRXBR-TB, J. T. Frasier
ATTN: Robert E. Eichelberger

Commander
US Army Mat. & Mechanics Research Center
ATTN: DRXMR-HH, John F. Dignam

Commander
US Army Materiel Dev. & Readiness Command
ATTN: DRCDE-D, Lawrence Flynn

Commander
US Army Missile Command
ATTN: DRSMI-XS, Chief Scientist

Commander
US Army Nuclear Agency
ATTN: MONA-WE
ATTN: MONA-SA

DEPARTMENT OF THE NAVY

Chief of Naval Material
Navy Department
ATTN: MAT 0323, Irving Jaffe

Chief of Naval Operations
Navy Department
ATTN: OP 981
ATTN: OP 62

Chief of Naval Research
Navy Department
ATTN: Code 464, Thomas P. Quinn

Director
Naval Research Laboratory
ATTN: Code 5180, Mario A. Persechino
ATTN: Code 7770, Gerald Cooperstein
ATTN: Code 2600, Tech. Lib.

Commander
Naval Sea Systems Command
Navy Department
ATTN: 0333A, Marlin A. Kinna

DEPARTMENT OF THE NAVY (Continued)

Commander
Naval Surface Weapons Center
ATTN: Code WA501, Navy Nuc. Prgms. Off.
ATTN: Code 2302
ATTN: Code 323, W. Carson Lyons

Director
Strategic Systems Project Office
Navy Department
ATTN: NSP-272

DEPARTMENT OF THE AIR FORCE

AF Materials Laboratory, AFSC
ATTN: MBC, Donald L. Schmidt
ATTN: MAS
ATTN: T. Nicholas

AF Rocket Propulsion Laboratory, AFSC
ATTN: RTSN, G. A. Beale

AF Weapons Laboratory, AFSC
ATTN: DYS
ATTN: DYT
ATTN: DYP
ATTN: DYV
ATTN: SUL

Commander
Foreign Technology Division, AFSC
ATTN: TDFBD, J. D. Pumphrey
ATTN: TDPTN

Hq. USAF/RD
ATTN: RDQ
ATTN: RDPM

SAMSO/DY
ATTN: DYS

SAMSO/MN
ATTN: MNNR

SAMSO/RS
ATTN: RSSE
ATTN: RSS

Commander in Chief
Strategic Air Command
ATTN: XPFS
ATTN: XOBM

ENERGY RESEARCH & DEVELOPMENT ADMINISTRATION

Division of Military Application
US Energy Research & Dev. Admin.
ATTN: Doc. Con. for Res. & Dev. Branch

University of California
Lawrence Livermore Laboratory
ATTN: Joseph E. Keller, Jr., L-125

Los Alamos Scientific Laboratory
ATTN: Doc. Con. for R. Dingus
ATTN: Doc. Con. for R. Skaggs

ENERGY RESEARCH & DEVELOPMENT ADMINISTRATION (Continued)

Sandia Laboratories
Livermore Laboratory
ATTN: Doc. Con. for Tech. Lib.
ATTN: Doc. Con. for 8131, H. F. Norris, Jr.
ATTN: Raymond Ng

Sandia Laboratories
ATTN: Doc. Con. for M. Cowan
ATTN: Doc. Con. for R. R. Boade

DEPARTMENT OF DEFENSE CONTRACTORS

Acurex Corporation
ATTN: J. Huntington

Aerospace Corporation
ATTN: Richard Crolius, A2-Rm. 1027
ATTN: W. Barry
ATTN: R. Strickler
ATTN: R. Mortensen

Avco Research & Systems Group
ATTN: John Gilmore, J400
ATTN: John E. Stevens, J100
ATTN: W. Broding, J200
ATTN: D. Henderson

Battelle Memorial Institute
ATTN: Tech. Lib.

The Boeing Company
ATTN: Brian Lempriere

California Research & Technology, Inc.
ATTN: Ken Kreyenhagen

Effects Technology, Inc.
ATTN: Robert Wengler

Ford Aerospace & Communications Operations
ATTN: P. Spangler

General Electric Company
Space Division
Valley Forge Space Center
ATTN: Carl Anderson
ATTN: Phillip Cline
ATTN: G. Harrison

General Electric Company
TEMPO-Center for Advanced Studies
ATTN: DASIAC

ION Physics Corporation
ATTN: Robert D. Evans

Kaman AviDyne
Division of Kaman Sciences Corp.
ATTN: Norman P. Hobbs

Kaman Sciences Corporation
ATTN: Frank H. Shelton
ATTN: Thomas Meagher

DEPARTMENT OF DEFENSE CONTRACTORS (Continued)

Lockheed Missiles & Space Company, Inc.
ATTN: Dept. 81-14, R. Walz

Lockheed Missiles & Space Company, Inc.
ATTN: F. G. Borgardt

Martin Marietta Aerospace
Orlando Division
ATTN: Laird Kinnaird

McDonnell Douglas Corporation
ATTN: L. Cohen
ATTN: J. F. Garibotti
ATTN: R. J. Reck
ATTN: E. A. Fitzgerald

Northrop Corporation
ATTN: Don Hicks

Physics International Company
ATTN: Doc. Con. for James Shea

Prototype Development Associates, Inc.
ATTN: John Slaughter

R & D Associates
ATTN: F. A. Field
ATTN: Jerry Carpenter
ATTN: Paul Rausch

DEPARTMENT OF DEFENSE CONTRACTORS (Continued)

Science Applications, Inc.
ATTN: G. Ray
ATTN: O. Nance

Southern Research Institute
ATTN: C. D. Pears

Stanford Research Institute
ATTN: George R. Abrahamson
ATTN: Herbert E. Lindberg
ATTN: J. D. Colton
ATTN: R. E. Emerson

Stanford Research Institute
ATTN: W. B. Reuland
ATTN: Harold Carey

Systems, Science & Software, Inc.
ATTN: G. A. Gurtman
ATTN: Russell E. Duff